Application of shallow and deep convolutional neural networks to recognize the average flow rate of physiological fluids in a capillary

Ivan Stebakov, Elena Kornaeva, Elena Potapova, Viktor Dremin

Ivan N. Stebakov, Elena P. Kornaeva, Elena V. Potapova, Viktor V. Dremin, "Application of shallow and deep convolutional neural networks to recognize the average flow rate of physiological fluids in a capillary," Proc. SPIE 12194, Computational Biophysics and Nanobiophotonics, 121940D (29 April 2022); doi: 10.1117/12.2626125

SPIE.

Event: XXV Annual Conference Saratov Fall Meeting 2021; and IX Symposium on Optics and Biophotonics, 2021, Saratov, Russian Federation

Application of shallow and deep convolutional neural networks to recognize the average flow rate of physiological fluids in a capillary

Ivan Stebakov[a,*], Elena Kornaeva[b], Elena Potapova[c], and Viktor Dremin[c,d]
[a]Department of Mechatronics, Mechanics and Robotics, Orel State University named after I.S.; Turgenev, Orel, 302026, Russian Federation; [b]Department of Information Systems and Digital Technologies, Orel State University named after I.S. Turgenev, Orel, 302026, Russian Federation; [c]Research and Development Center of Biomedical Photonics, Orel State University named after I.S. Turgenev, Orel, 302026, Russian Federation; [d]College of Engineering and Physical Sciences, Aston University, Birmingham, B4 7ET, United Kingdom

ABSTRACT

The aim of this work is to develop practical tools to recognize the average flow rate of physiological fluids in capillaries. This tool is represented by classification models in an artificial neural networks form. The flow rate data were obtained experimentally. Intralipid was used as the test liquid. Laser speckle contrast imaging was used to obtain images of liquid flow in a glass capillary. The experiment was carried out with an average flow rate of 0-2 mm/s with various concentrations of intralipid. The results of training of fully connected and convolutional neural networks for processing the received data are presented. The accuracy of determining the average flow rate of intralipid with different concentrations was comparable to the previously obtained results for a fixed concentration and amounted to approximately 97.5%.

Keywords: physiological fluid, flow rate, rheology, laser speckle contrast imaging, artificial neural network

1. INTRODUCTION

The rheological properties of physiological fluids can perform a diagnostic function in determining pathological conditions in a wide range of diseases [1–3]. In particular, blood viscosity is an important hemorheological parameter that affects blood flow and circulation. Monitoring changes in blood viscosity can become an important tool for diagnosing and predicting hemorheological changes [4,5]. For example, increased blood viscosity is associated with several pathological conditions, such as sickle cell anemia and diabetes mellitus, which can contribute to vascular complications and impaired tissue perfusion [6,7].

Non-invasive diagnostic methods are of particular interest. Ref. [8]discusses that dynamic light scattering methods can be used to register kinematic parameters of physiological fluid flow. Thus, significant advances have been made in the application of laser Doppler flowmetry (LDF) [9] and laser speckle contrast imaging (LSCI) [10], which allow *in vivo* studies.

The development of machine learning (ML) methods, in particular deep learning, as well as modern ways to speed up computations, allow to develop complex models based on big data analysis. Thus, in [11], a model is presented for the diagnosis of acute leukemia based on the processing of images of blood cells by a convolutional neural network. In [12], various machine learning models are used to detect skin cancer by polarization speckle.

The model based on feed-forward artificial neural network (ANN) is presented in Ref. [13]. This model makes it possible to determine the average flow rate of intralipid of fixed concentration, which approximately corresponds to the optical scattering properties of blood. However, the value of speckle contrast changes due to changes in the properties of optical scattering when studying the flow of various intralipid concentrations by the LSCI method. As a result, this makes it difficult to estimate the fluid velocity.

This article discusses the average flow rate recognizing problem of physiological fluids using ANN. For recognition, the images of the intralipid solution flow in the channel obtained by the LSCI method are used. The main difficulty is that different intralipid concentrations affect the optical scattering properties.

*chester50796@yandex.ru; phone +7 953 618 08 66

Computational Biophysics and Nanobiophotonics, edited by Dmitry E. Postnov, Boris N. Khlebtsov,
Proc. of SPIE Vol. 12194, 121940D · © 2022 SPIE · 1605-7422 · doi: 10.1117/12.2626125

2. EXPERIMENTAL SETUP

The aim of this work is to research the influence of the intralipid concentration, and the camera positioning on the flow rate. The study was implemented with the experimental setup that combines the fluid flow circuit and the LSCI equipment (see Fig. 1), designed earlier [10,14,15]. The enforced fluid flow through the medical glass capillary with a diameter of 1.6 mm was investigated. The studied fluid is 20 % intralipid (Fresenius Kaby, USA). The electric pump DSh-08 (Visma, Belarus) provides a flow rate of a known value, while the UI-3360CP-NIR-GL Rev.2 (IDS GmbH, Germany) CMOS camera combined with the extension adapter and MVL25TM23 lens (Thorlabs, Inc., USA) records the intralipid flow illuminated by a 785 nm laser (LDM785, Thorlabs Inc.).

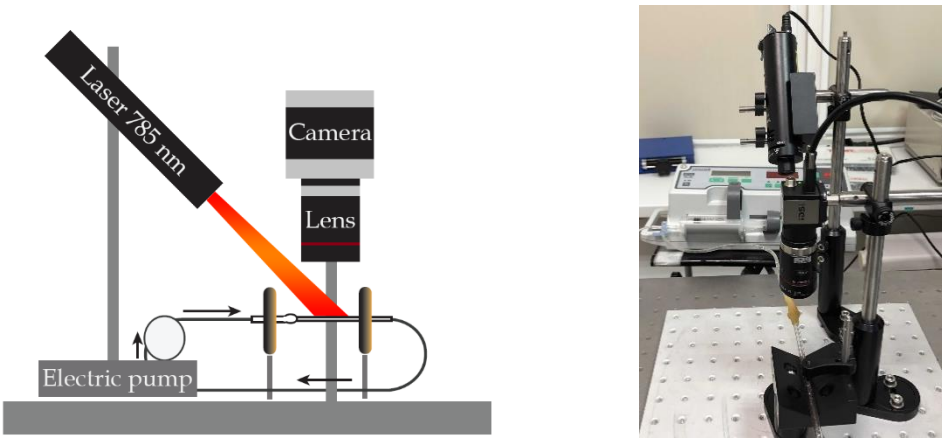

a) b)

Figure. 1. The experimental setup: schematic (a) and photograph (b)

The study plan consisted of 75 tests including 5 parallel tests at each combination of factors. The tests were performed in random order. Each test lasted 1 minute. The camera recorded the flow with the resolution of 2048×512 pixels at the frequency of 30 FPS. The flow rate was of 0, 0.5, 1, 1.5, and 2 mm/s. The intralipid was diluted to concentrations of 4, 8, and 12 %. The camera exposition time was 15.

3. METHODOLOGY

3.1 Laser speckle contrast imaging

By analyzing the local speckle contrast, the LSCI method allows one to obtain an image of dynamic inhomogeneities [16]. When the scattering medium is illuminated with coherent radiation, a random picture of the light intensity arises. This pattern is caused by interference within the medium and at its surface. The resulting intensity structure is known as a speckle pattern. The movement of particles in the medium leads to blurring in the image due to averaging over the exposure time of the camera. Spatial and temporal statistics of speckle patterns are used to extract information about movement in the environment under study. Spatial speckle contrast (SSC) is calculated in a small square area of the image. The optimal size for this area is a 7×7 pixel window. This window moves horizontally and vertically across the image. The spatial speckle contrast in each window is calculated using the formula:

$$K = \frac{\sigma_n}{\langle I_n \rangle}, \tag{1}$$

where n is the calculation domain size; σ_n is the intensity standard deviation; $\langle I_n \rangle$ is mean intensity.
The K value ranges from 0 to 1. Temporal speckle contrast (TSC) is used to calculate the intensity value in one pixel of several frames. Space time speckle contrast (STSC) combines the areas previously described.

3.2 Artificial neural networks

This article uses supervised learning to solve the average flow rate classification problem. Artificial neural networks (ANNs) are used for this problem. The model being trained must determine the relationship between the input set and the

target set of classes $\boldsymbol{Y} = \left(\left(\boldsymbol{y}^{(1)}, \ldots, \boldsymbol{y}^{(m)}\right)\right)$ by finding the parameter values $\boldsymbol{\Theta} = \left(\left(\boldsymbol{\Theta}^{(1)}, \ldots, \boldsymbol{\Theta}^{(l)}\right)\right)$, where m – is the sample index, l – is the neural network layer index. This model is a complex function that defines a set of predictions of probabilities $\boldsymbol{H} = \boldsymbol{H}(\boldsymbol{X}, \boldsymbol{\Theta})$. Data arrays of arbitrary shape are used as samples of the input and target sets.

The cross-entropy loss is used as an error function [17]:

$$L(\Theta) = -\sum_{i=1}^{m}\sum_{j=}^{n_l}\left(\tilde{y}_j^{(i)} \ln(h_j^{(i)})\right) \Rightarrow \min, \tag{2}$$

where $h_j^{(i)}$ is predicted for a given input $\boldsymbol{X}^{(i)}$ probability of being assigned to an j-th class, $\tilde{y}_j^{(i)}$ is a target value for a given input $\boldsymbol{X}^{(i)}$ of being assigned to an j-th class ($\tilde{y}_j^{(i)} = 1$ if j corresponds to the number of the class, and $\tilde{y}_j^{(i)} = 0$ otherwise), n_l is the number of neurons in the output layer of ANN that is equal to the number of classes.

ANN computations are of two types: forward propagation to obtain predictions and back propagation to obtain gradient components$((L'_\theta))$of the error function. Back propagation is performed to implement a gradient descent method that minimizes the error value L and finds the best values for the parameters $\boldsymbol{\Theta}$. In this paper, we use a version of the Adam's method [18].

The most common neural network is the multilayer perceptron (MLP), which consists of several fully connected layers (Fig. 2). The value of neurons in these layers is determined by a non-linear activation function. The argument of this function is the weighted sum of the neurons of the previous layer. In this work, the ReLU function is used as the activation function for the hidden layer. The input layer takes the values of set X, the samples of which are vectors. The output layer is used to predict a specific class using the SoftMax activation function. Also, before activation, a Batch Normalization layer is used, which avoids overfitting. When applying this layer, the bias parameter is used only in the output layer. This technique helps to increase the accuracy of deep learning models [19].

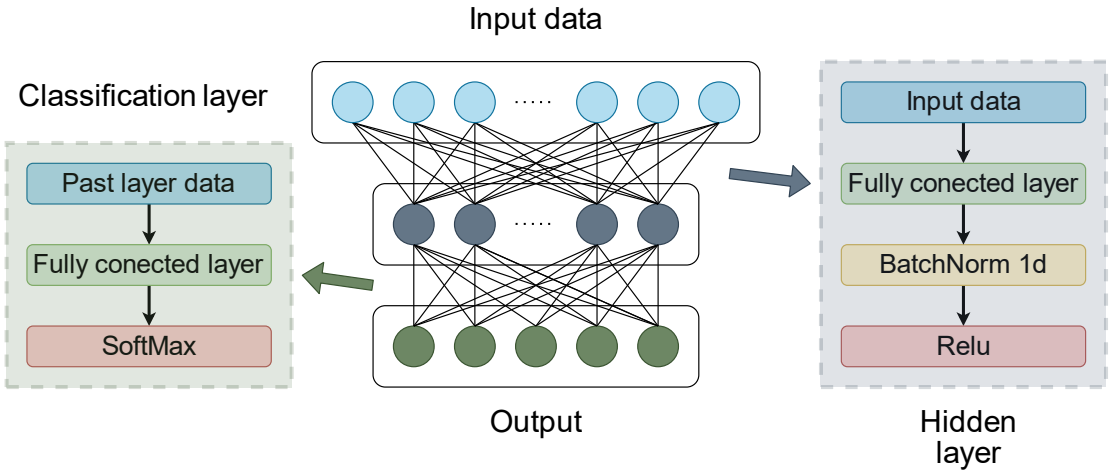

Figure 2. Architecture of the MLP

The convolutional neural network (CNN) was originally developed for image processing. They compress pixel intensity data and highlight important features. The convolution operation is the complete dot product of the fragments of the input image and the corresponding kernel. The kernel components are included in the set of network parameters $\boldsymbol{\Theta}$ and their values are determined during training. The convolutional layers also use padding to control the size of the output and stride to reduce the dimension of the data. The number of kernels in the convolutional layer determines the number of output channels. After the convolution operation, the Batch Normalization layers and activation functions are also applied. For classification, the CNN output is processed by one or more fully connected layers such as MLP.

In this work, we use the CNN ResNet18 [20] (Fig. 3). The peculiarity of the ResNet architecture is the shortcut connections. The Stride in the layers of the network is 2. ResNet 18 accepts an image of arbitrary size and three channels as input.

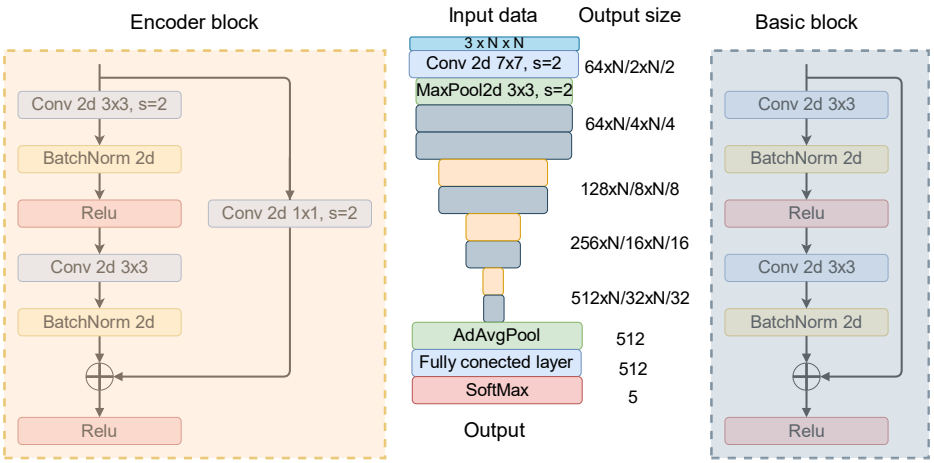

Figure 3. Architecture of ResNet18

The PyTorch library was used to train the proposed models [21]. To speed up the calculations, a GeForce 1660 TI video card with CUDA driver support was used.

4. RESULTS

4.1 Data preparation

The first results were obtained for a concentration of 8%. The accuracy of resulting shallow ANN model was about 88.5% and that exceed the accuracy of experts. Spatial speckle contrast averaged over 120 frames (mean SSC) was the best method for preparing the data. Using this method, the resulting model became resistant to pulsations of the pump used in the experiment. The disadvantage of the developed model is that it allows to recognize the flow rate of liquid with a constant concentration [13]. Thus, the main challenge in this work is the development of a model capable of recognizing the flow rate of a liquid with varying reflective properties.

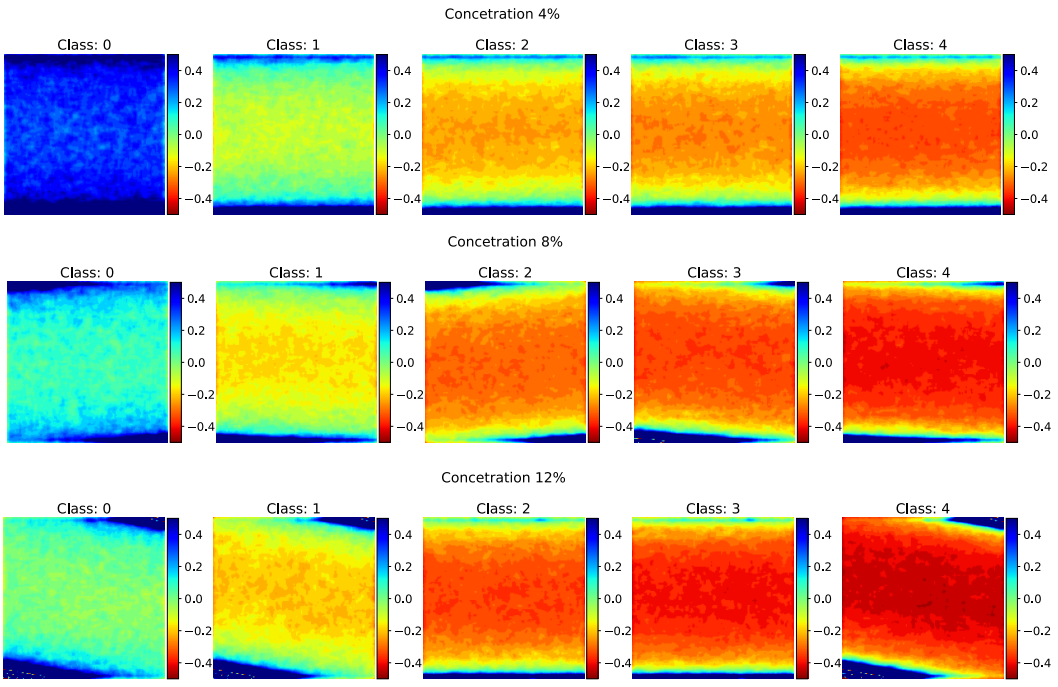

Figure 4. Training images represent the capillary central part domain of 160×160 pixels

The data were pre-cleared of outliers. The images for training were obtained using the mean SSC algorithm. These images were cropped to a size of 160×160 pixels so that the center of the capillary is in the center of the resulting image. The dataset was divided into 3 parts: 68947 samples for training, 24851 for validation, and 23427 for test. Figure 4 shows examples of images for each class and concentration. Standard scale normalization was applied for the training examples.

Figure 5 shows the average mean SSC values in the capillary central part domain of 40×40 pixels on 120 frames. It can be seen that as the speed increases, the value of the speckle contrast decreases. However, the amount of speckle contrast also changes with concentration, making it difficult to analyze the images.

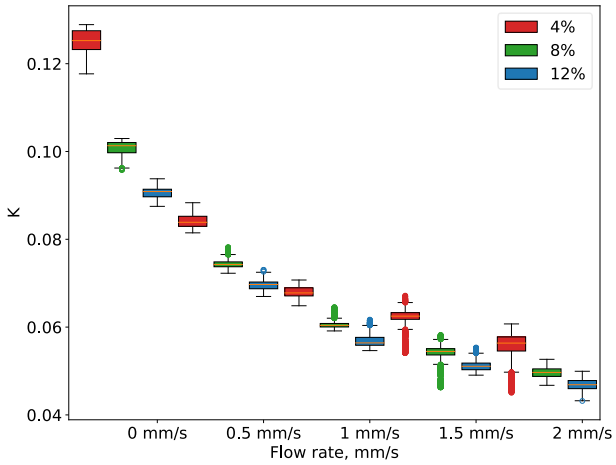

Figure 5. Speckle contrasts calculated in the capillary central part domain of 40×40 pixels at the different fluid flow rates and concentrations using mean SSC

4.2 Comparison of architectures

The shallow ANN was trained with different number of hidden neurons: $l_{hid} = [8,16,32,64]$. The learning rate and the regularization parameter value were also varied in shallow ANN and ResNet 18. The parameters were selected based on the validation results. Table 1 shows that the ResNet 18 accuracy is higher than the shallow ANN accuracy. The best accuracy for the test set was 88.8%. Figure 6 demonstrates ResNet 18 confusion matrices.

Table. 1. The ANN and ResNet 18 results

Model	Training accuracy	Validation accuracy	Test accuracy
Multilayer Perceptron	0.9978	0.9919	0.8382
ResNet 18	0.9942	**0.9988**	**0.8884**

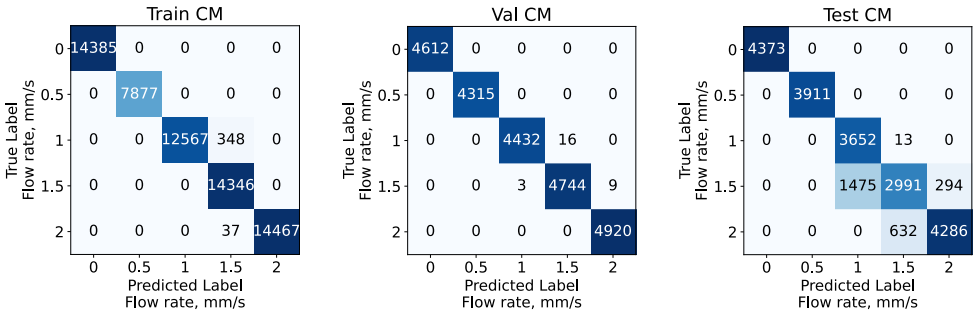

Figure 6. The ResNet 18 confusion matrices

4.3 Ensemble of models

To increase the recognition accuracy, an ensemble of several models is used. For this, the training data was divided into 4 folds. Each of them was used for validation on the corresponding model. The rest of the data were used for training. The test sample remained unchanged. Table 2 shows the learning results for different folds. Figure 7 demonstrates ensemble confusion matrices.

Table. 2. The ensemble results

Model	Training accuracy	Validation accuracy	Test accuracy
FOLD 1	0.9976	0.9977	0.8860
FOLD 2	0.9813	0.9553	0.9369
FOLD 3	1.0000	0.9484	0.9113
FOLD 4	0.9754	0.9353	0.9299
Ensemble	0.9869		0.9759

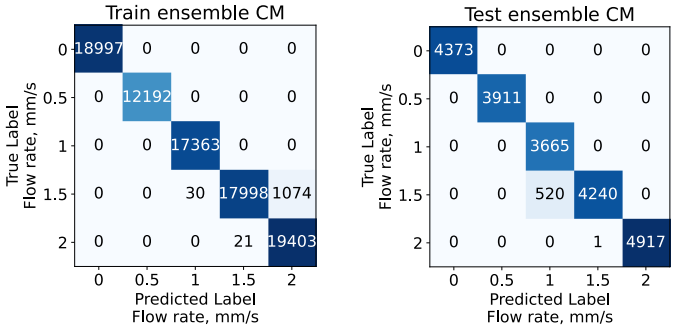

Figure 7. The ensemble confusion matrices

The precision of the ensemble in the test set was 97.59%. The F1-score metric for each class was, respectively: 100%, 100%, 93.38%, 99.99%. The average F1-score is 97.52%. Therefore, the recognition accuracy of the average intralipid flow rate with different concentrations was comparable to the accuracy of a fixed concentration.

5. CONCLUSIONS

The best accuracy and F1 score are about 97.5% for the test sample was obtained for the case of using the ensemble of ResNet 18 models. The developed algorithm and model made it possible to determine the average flow rate of a solution of intralipid of various concentrations. In addition, the algorithm proved to be resistant to pulsation of the pump used in the experiment. The combination of LSCI and machine learning techniques to study the flow of body fluids holds promise for many applications, including health monitoring and diagnostics. Further research will aim to create a compact device for measuring the viscosity of physiological fluids. The device will allow to automate calculations of viscosity based on the use of deep neural networks. Training data will be received on the same device using the LSCI method. Thus, the device will make it possible to diagnose the state of cells of physiological fluids in real time.

ACKNOWLEDGEMENTS

This work was supported by the Russian Science Foundation under the Project 20-79-00332. The authors gratefully acknowledge this support.

CREDIT AUTHORSHIP CONTRIBUTION STATEMENT

E. Kornaeva and V. Dremin proposed the ANN and the speckle contrast imaging mathematical models in section 3, respectively. I. Stebakov designed the algorithm, wrote the program code, tested it, and analyzed the experimental data. E. Potapova designed the test setup. I. Stebakov performed the experiment. I. Stebakov and E. Kornaeva wrote the manuscript.

REFERENCES

[1] Xu, J., Vilanova, G., and Gomez, H., "Phase-field model of vascular tumor growth: Three-dimensional geometry of the vascular network and integration with imaging data," Computer Methods in Applied Mechanics and Engineering 359, 112648 (2020).

[2] Priezzhev, A. v., Semenov, A.N., Lugovtsov, A.E., Lee, K., Fabrichnova, A.A., and Kovaleva, Yu.A., "Applying Methods of Diffuse Light Scattering and Optical Trapping for Assessing Blood Rheological Parameters: Erythrocytes Aggregation in Diabetes Mellitus," Series Physics 17(2), 85–97 (2017).

[3] Yeow, N., Tabor, R.F., and Garnier, G., "Atomic force microscopy: From red blood cells to immunohaematology," Advances in Colloid and Interface Science 249, 149–162 (2017).

[4] Sugimori, H., Tomoda, F., Koike, T., Kurosaki, H., Masutani, T., Ohara, M., Kagitani, S., and Inoue, H., "Increased blood viscosity is associated with reduced renal function and elevated urinary albumin excretion in essential hypertensives without chronic kidney disease," Hypertension Research 2013 36:3 36(3), 247–251 (2012).

[5] Tamariz, L.J., Young, J.H., Pankow, J.S., Yeh, H.-C., Schmidt, M.I., Astor, B., and Brancati, F.L., "Blood Viscosity and Hematocrit as Risk Factors for Type 2 Diabetes MellitusThe Atherosclerosis Risk in Communities (ARIC) Study," American Journal of Epidemiology 168(10), 1153–1160 (2008).

[6] Johnson, C.S., "Arterial Blood Pressure and Hyperviscosity in Sickle Cell Disease," Hematology/Oncology Clinics of North America 19(5), 827–837 (2005).

[7] Cho, Y.I., Mooney, M.P., and Cho, D.J., "Hemorheological Disorders in Diabetes Mellitus," Journal of Diabetes Science and Technology 2(6), 1130–1138 (2008).

[8] Dremin, V. v., Zherebtsov, E.A., Makovik, I.N., Kozlov, I.O., Sidorov, V. v., Krupatkin, A.I., Dunaev, A. v., Rafailov, I.E., Litvinova, K.S., et al., "Laser Doppler flowmetry in blood and lymph monitoring, technical aspects and analysis," Proceedings Volume 10063, Dynamics and Fluctuations in Biomedical Photonics XIV 10063, 2–9 (2017).

[9] Stavtsev, D.D., Volkov, M. v., Margaryants, N.B., Potemkin, A. v., Dremin, V. v., Kozlov, I.O., Makovik, I.N., Zherebtsov, E.A., and Dunaev, A. v., "Investigation of blood microcirculation parameters in patients with rheumatic diseases by videocapillaroscopy and laser Doppler flowmetry during cold pressor test," Proceedings Volume 11065, Saratov Fall Meeting 2018: Optical and Nano-Technologies for Biology and Medicine 11065, 189–194 (2019).

[10] Potapova, E.V., Seryogina, E.S., Dremin, V.V., Stavtsev, D.D., Kozlov, I.O., Zherebtsov, E.A., Mamoshin, A.V., Ivanov, Yu.V., and Dunaev, A.V., "Laser speckle contrast imaging of blood microcirculation in pancreatic tissues during laparoscopic interventions," Quantum Electronics 50(1), 33 (2020).

[11] Boldú, L., Merino, A., Acevedo, A., Molina, A., and Rodellar, J., "A deep learning model (ALNet) for the diagnosis of acute leukaemia lineage using peripheral blood cell images," Computer Methods and Programs in Biomedicine 202, (2021).
[12] Wang, Y., Louie, D.C., Cai, J., Tchvialeva, L., Lui, H., Jane Wang, Z., and Lee, T.K., "Deep learning enhances polarization speckle for in vivo skin cancer detection," Optics and Laser Technology 140, (2021).
[13] Stebakov, I., Kornaeva, E., Stavtsev, D., and Potapova, E., "Laser speckle contrast imaging and machine learning in application to physiological fluids flow rate recognition," Vibroengineering Procedia 38, 50–55 (2021).
[14] Mizeva, I., Dremin, V., Potapova, E., Zherebtsov, E., Kozlov, I., and Dunaev, A., "Wavelet Analysis of the Temporal Dynamics of the Laser Speckle Contrast in Human Skin," IEEE Transactions on Biomedical Engineering 67(7), 1882–1889 (2020).
[15] Dremin, V., Potapova, E., Mamoshin, A., Dunaev, A., and Rafailov, E., "Monitoring oxidative metabolism while modeling pancreatic ischemia in mice using a multimodal spectroscopy technique," Laser Physics Letters 17(11), 115605 (2020).
[16] Draijer, M., Erwin, ·, Ton Van Leeuwen, H.·, and Steenbergen, W., "Review of laser speckle contrast techniques for visualizing tissue perfusion," Lasers Med Sci 24, 639–651 (2009).
[17] "BCELoss — PyTorch 1.10.0 documentation," <https://pytorch.org/docs/stable/generated/torch.nn.BCELoss> (6 November 2021).
[18] Kingma, D.P., and Lei Ba, J., "ADAM: A METHOD FOR STOCHASTIC OPTIMIZATION."
[19] Ian Goodfellow and Yoshua Bengio and Aaron Courville, [Deep Learning] , MIT Press (2016).
[20] He, K., Zhang, X., Ren, S., and Sun, J., "Deep Residual Learning for Image Recognition."
[21] "PyTorch," <https://pytorch.org/> (6 November 2021).